ORNL/TM-2022/2663

Small Punch Testing of Molybdenum-99 Targets

Holden C. Hyer

September 2022

Approved for public release.
Distribution is unlimited.

OAK RIDGE National Laboratory

ORNL IS MANAGED BY UT-BATTELLE LLC FOR THE US DEPARTMENT OF ENERGY

ORNL/TM-2022/2663

Nuclear Energy and Fuel Cycle Division

SMALL PUNCH TESTING OF MOLYBDENUM-99 TARGETS

Holden C. Hyer

September 2022

NorthStar Accelerator Milestone #A9D1

Prepared by
OAK RIDGE NATIONAL LABORATORY
Oak Ridge, TN 37831
managed by
UT-BATTELLE LLC
for the
US DEPARTMENT OF ENERGY
under contract DE-AC05-00OR22725

CONTENTS

LIST OF FIGURES

LIST OF TABLES

ACKNOWLEDGMENTS

Support for this work was provided by the US Department of Energy's National Nuclear Security Administration, Office of Material Management and Minimization's Molybdenum-99 Program.

ABBREVIATIONS

aMo	^{100}Mo
CC	Calchemist
DOE	US Department of Energy
EBS	ethylene bis stearamide
HD	higher density
OD	outer diameter
ORNL	Oak Ridge National Laboratory
P_M	maximum load
$P_{t/10}$	load at $t/10$
P_Y	yield load
SA	stearic acid
SAW	stearic acid wiped
SPT	small punch test
SS	stainless steel
T	Teflon
t	thickness
UTS	ultimate tensile strength
YS	yield strength
δ_M	displacement at maximum load

EXECUTIVE SUMMARY

Northstar Medical Radioisotopes is developing an accelerator-based method to produce ^{99}Mo, which is a parent isotope of the commonly used ^{99m}Tc medical isotope. The Mo targets being designed for the accelerator will be produced from enriched ^{100}Mo, also known as *aMo*. Pressed and sintered powder feedstock is used to fabricate aMo targets, producing 29 mm disk-shaped targets. The targets are subjected to 1–6 days in line of an electron beam with subsequent dissolution of the disk to retain the ^{99}Mo, which decays to ^{99m}Tc at radio-pharmacies. The press and sinter method is advantageous because the inherent porosity produced by this method enables increased surface area and therefore increased flow of dissolution media, decreasing the dissolution time and reducing the need for a highly acidic media. Although porosity aids in dissolution, it reduces the mechanical strength and ductility. Targets require good mechanical integrity when subjected to the conditions in the accelerator. Therefore, Northstar is seeking methods to rapidly test disk samples after fabrication to assure mechanical performance metrics are achieved.

This report details the design and testing of a small punch test (SPT) that accommodates the 29 mm disk. Initial data were used to relate the SPT data to tensile properties, such as the yield strength (YS), ultimate tensile strength (UTS), and total elongation to failure. Although the SPT has been established as a somewhat reliable method for testing metallic materials, few studies have applied the SPT to refractory materials such as Mo. Based on tensile testing performed at Oak Ridge National Laboratory on different Mo samples, correlation between the Mo tensile and SPT properties could be performed, establishing a standard calibration that could be applied to other Mo samples. To test the efficacy of the SPT with Mo, multiple different disk batches were fabricated under different conditions (e.g., pressure, lubricant) with commercially available pure Mo powder. Generally, only a UTS could be well defined because the press and sinter disks failed under brittle fracture, making it difficult to determine the YS and elongation. Compared with disks fabricated with aMo powder, the aMo samples underperformed their pure ^{nat}Mo counterparts. This report summarizes the current status of the SPT, but further evaluation is needed before it can be applied as a reliable quality assurance tool.

1. INTRODUCTION

One of the most common medical isotopes used worldwide is ^{99m}Tc, a daughter isotope of ^{99}Mo [1]. After a patient is injected with a blend of ^{99m}Tc, customized to reside in specific locations in the body, those locations emit low-activity gamma rays, that are easily detected from outside the body. The energy is computer enhanced to create images for analysis. ^{99m}Tc rapidly decays with a half-life of 6 h, so it does not remain in the body for more than 1 week [1]. As a consequence of the short half-life hospitals and radiopharmacies need a continuous supply. Companies like Northstar have or are in the process of developing methods for producing reliable sources of ^{99}Mo to meet the nation's demand of ^{99m}Tc [2]. The National Nuclear Security Administration (NNSA) is supporting this endeavor to make the United States competitive for ^{99}Mo production without the use of highly enriched uranium (HEU) [2, 3]. Northstar is currently developing an accelerator-based strategy that employs an electron beam accelerator targeting a ^{100}Mo metallic target or *aMo*, targets [2]. The accelerated electron beam will be directed toward a tungsten (W) window, producing X-rays that then hit the aMo target and knock off one neutron to make ^{99}Mo. The aMo targets will be stacked into a holder designed with He flow in between each target for heat rejection [4, 5]. Therefore, these targets will be subjected to a thermal-pneumatic conditions necessitating the understanding of the aMo target's mechanical performance.

Currently, the design of the aMo target has a disk geometry with a total diameter of 29 mm and a thickness of 0.5 mm, including tight tolerances in average height [4]. Typically, most Mo products are fabricated from powder feedstock. The supply of aMo is similar to pure ^{nat}Mo because it is produced in powder form. Currently, aMo is manufactured into a target via the press and sinter method. Because there is typically unavoidable porosity, making it difficult to achieve a fully dense material, pressing and sintering Mo powder is not an ideal process compared with hot pressing, rolling, or arc casting in conventional methods [6, 7]. Once the target has been exposed to the accelerator, it is dissolved in a peroxide solution to ease the process of extracting the ^{99}Mo and, later, to rapidly generate into ^{99m}Tc [8]. Although porosity may hinder mechanical performance, it serves as a point of entry for increased dissolution, decreasing the corrosivity of the dissolution bath needed and the time it takes for full dissolution to be achieved.

Previous work was performed to understand the pressure, temperature, and time needed to make the targets from commercially sourced Mo powder [6, 9]. Moreover, thermal modeling was used to inform what mechanical and thermal loads are expected when the target is in line with the accelerator [5, 10, 11]. Therefore, thermal and mechanical testing of the samples are both desired to understand how the chosen geometry and manufacturing method will perform once in application. Producing larger specimens for mechanical behavior evaluation via tensile testing or other more common techniques may prove difficult and not be representative of sample size or the type of mechanical loads the targets are expected to be subjected to in the accelerator. This report briefly describes a method for testing the Northstar disk geometries via a custom designed small punch test (SPT) that can be used to evaluate the target disks themselves without any needed machining or special fabrication. This report provides data on the preliminary testing of disks manufactured from various lots of pure Mo powder, as well as the intended aMo powder.

2. EXPERIMENTAL METHODS

2.1 PUNCH TEST DESIGN

Tensile testing is the standard practice for measuring mechanical properties because it can be relatively easy to perform and provides some data that can be used to inform models. To perform a tensile test, samples must be fabricated into a dog-bone shape so that the force while pulling in tension is focused to the sample center, reducing potential anomalous fracture along the length of monolithic sample pulled in a similar fashion. However, fabricating the dog bone may be difficult for small amounts of material such as those used to manufacture aMo disks. Therefore, alternative tests that can apply local deformation to a sample without special machining or fabrication procedures, such as the SPT, are often preferred.

The SPT is summarized in ATSM E3205-20 [12] for use with metallic materials. Testing can be used to derive tensile properties, such as yield strength (YS), ultimate tensile strength (UTS), and effective elongation. This test was originally designed for exploring the ductile to brittle transition of metals and is approved for operation between approximately –200 to 450°C. However, many studies have used the test to rapidly evaluate the tensile properties from a small amount of material in a relatively simple geometry (e.g., a disk) rather than have a dog-bone type specimen machined for tensile testing. A typical punch test setup is shown in Figure 1(a), whose labels are described in Table 1.

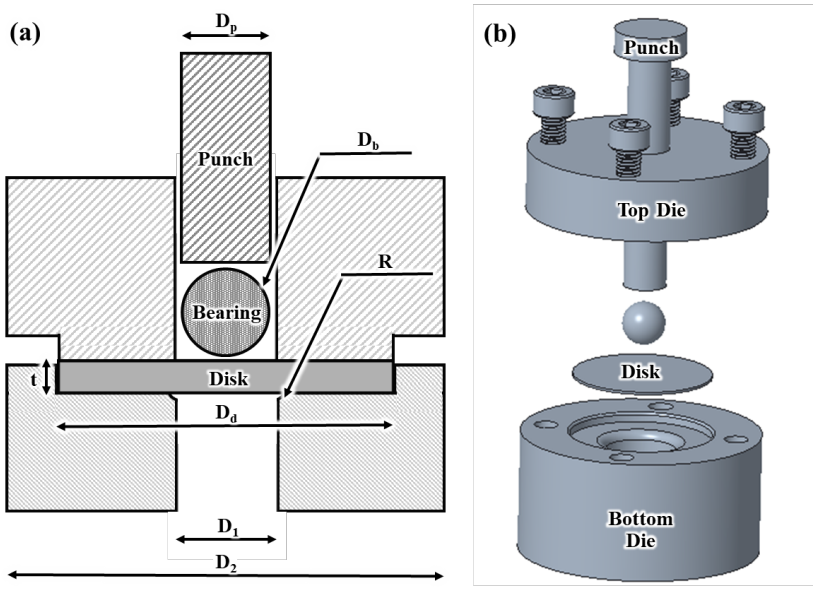

Figure 1. (a) Schematic and (b) drawing of the SPT.

Table 1. List of symbols and their corresponding description for the schematics shown in Figure 1(a).

Symbol	Description
D_p	Punch
D_b	Ball bearing
D_d	Disk specimen
D_1	Die rest
D_2	Die total
t	Disk thickness
R	Rest radius
P_Y	Load at yield
$P_{t/10}$	Load at 1/10 the sample thickness
P_M	Maximum load achieved
$\delta_{t/10}$	Deflection 1/10 the sample thickness
δ_M	Deflection at maximum load

For the SPT, the test specimen is usually a disk with a given thickness, t, that is sandwiched between two dies to ensure the sample moves as little as possible. Full details on the different dimensions are reported in Table 1. Punching is performed with hemispherical surface, usually a ball bearing driven by a punch, to drive the sample through a hole. The ASTM standard [12] is written for a small disk with an outer diameter (OD) of 8 mm and a thickness of 0.5 mm. To accommodate the 29 mm OD disks based on the aMo target design, a new set of dies with larger dimensions was used. Using a simple sizing ratio, the new dimensions were drafted based on the 29 mm OD disk and are reported in Table 2. A 3D drawing of the new die setup is shown in Figure 1(b). The dies were machined from D2-Tool steel with Rockwell C hardness of 60, which is above the 55 hardness limit suggested by the ASTM standard [12].

Table 2. SPT die dimensions used for the 29 mm OD disks compared with the dimensions of the 8 mm OD disk provided by the ASTM E3205-20 standard [12].

Symbol/ description	ASTM recommended dimensions (mm)	Dimensions by ratio with disk (mm)	Drawing dimensions (mm)
Disk diameter, D_d	8	29	29
Disk thickness, t	0.5	1.84	0.5
Rest radius, R	0.2	0.74	0.75
Bearing diameter, D_b	2.5	9.22	9
D_1	8	29.5	29.5
D_2	4	14.75	14.75

2.2 MECHANICAL TESTING

2.2.1 Test Setup

A simple procedure was adopted to ready the dies shown in Figure 1(b) for mechanical testing. The disks should easily fit into the recessed slot in the bottom die, shown in Figure 2(a), but if the disk is not completely flat, then it will likely not fit in the recess. Disks with slightly smaller ODs should be inserted with a thin shim that can fit around the disk and maintain the centered location. After the disk is loaded, it is covered with the top die (Figure 2[b]), and the dies are held together with four cap screws (Figure 2[c]). As the screws are tightened, the top die must remain level with the bottom die (Figure 2[d]), regardless of whether the disk is warped. If the disk is warped, the screws are driven with only a minimal amount of force. A torque wrench set at 2 in-lb, is applied to finish tightening all the screws. If the sample is brittle,

then less torque is used to reduce the changes of premature fracture. Large torques of 5–10 in-lb are used for harder and more ductile samples to ensure that samples do not move during testing. Finally, the ball bearing is inserted and ready to punch, as shown in Figure 2(e).

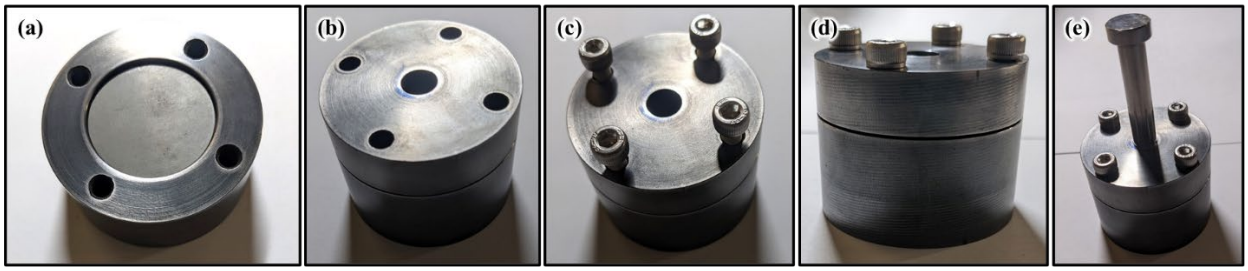

Figure 2. General flow in setting up a die for testing. The process includes (a) inserting the disk, (b) placing the top die on gently, (c) placing the four screws, (d) screwing each screw while maintaining a level surface, and then (e) inserting the ball bearing and punch. Then, the setup can be inserted into the testing frame.

The testing performed in this report was done with an in-house tensile-compression MTS™ load frame. The load cell used was 25 kN with an MTS 407 controller. A crosshead compression rate of 0.025 mm/s was used for the testing. The sensitivity of the controller is high enough that no additional displacement bars or extensometers were used. The rate of collection was set at 10 points/second. Each test was taken to first failure after the maximum load was achieved before stopping and resetting for the next test. Some tests were continued to observe any possible reloading of the sample.

2.2.2 SPT Loading Behavior

During a SPT, a punch is driven toward a disk sample, often with a press or testing frame. For full understanding of the mechanical behavior during the SPT, the dies are typically setup in a tensile-compressive frame so that the force and displacement can be measured. The typical load vs. displacement curve of a ductile sample subjected to SPT is shown in Figure 3(a) [13]. A stress-strain curve typically derived from a tensile test cannot be reproduced with the SPT. Therefore, specific data must be extracted to relate the behavior observed in the SPT to tensile properties. The unique values that are extracted include the load at yield (P_Y), maximum load (P_M), and displacement at maximum load (δ_M) [13]. The P_Y is often not representative of the material load at yield. Similar to a 0.02% offset performed to determine YS in the elastic region of a tensile stress-strain curve, the load ($P_{t/10}$) at 1/10 the thickness ($\delta_{t/10}$) of the sample is most representative of the sample's yield load. This requires drawing a line with the same slope at the elastic region with an x-intercept at the $\delta_{t/10}$, as shown in Figure 3(a) [13-15].

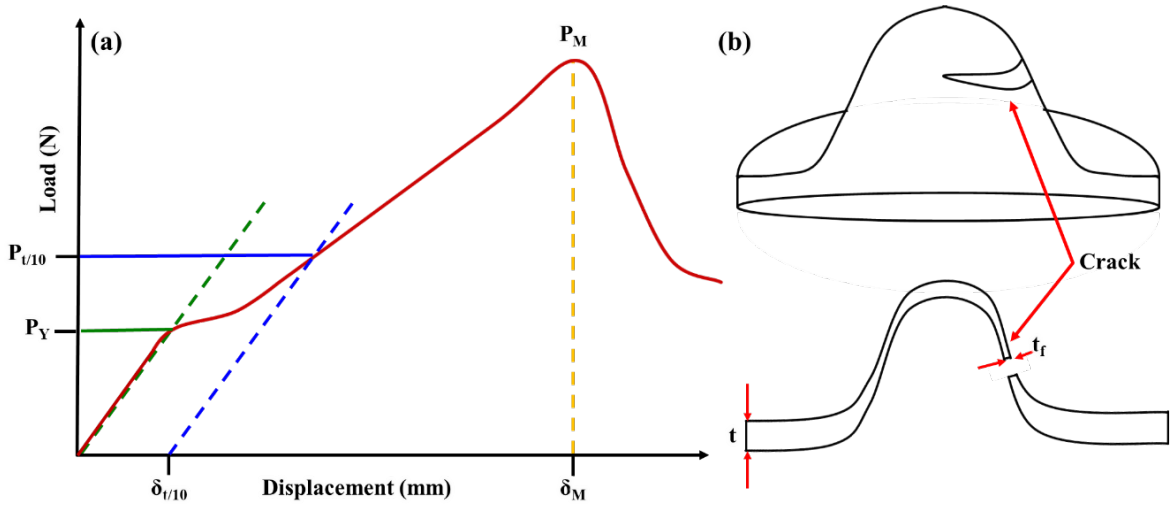

Figure 3. Schematics of the typical (a) load vs. displacement curve for a SPT disk sample and (b) fracture mechanism of a ductile disk sample.

3. RESULTS AND ANALYSES

3.1 SAMPLE BATCHES AND SPT LOADING

Preliminary tests were performed on sheet Mo manufactured from a combination of powder metallurgy with subsequent high-temperature forging operations. Disks with a 29 mm OD were punched flat with a given thickness of 0.5 mm. The sheet Mo has a part density of <99% and should be most representative of pure Mo. The high density was achieved through consecutive hot rolling of compacted Mo powder. SPT results from one of the sheet Mo disks are shown in Figure 4. The curve is similar to the ideal curve from an SPT test shown in Figure 3(a). An indication should exist at low displacement of the yield point where the slope of the curve changes. Once the maximum load is reached, the sample is usually expected to experience its initial fracture.

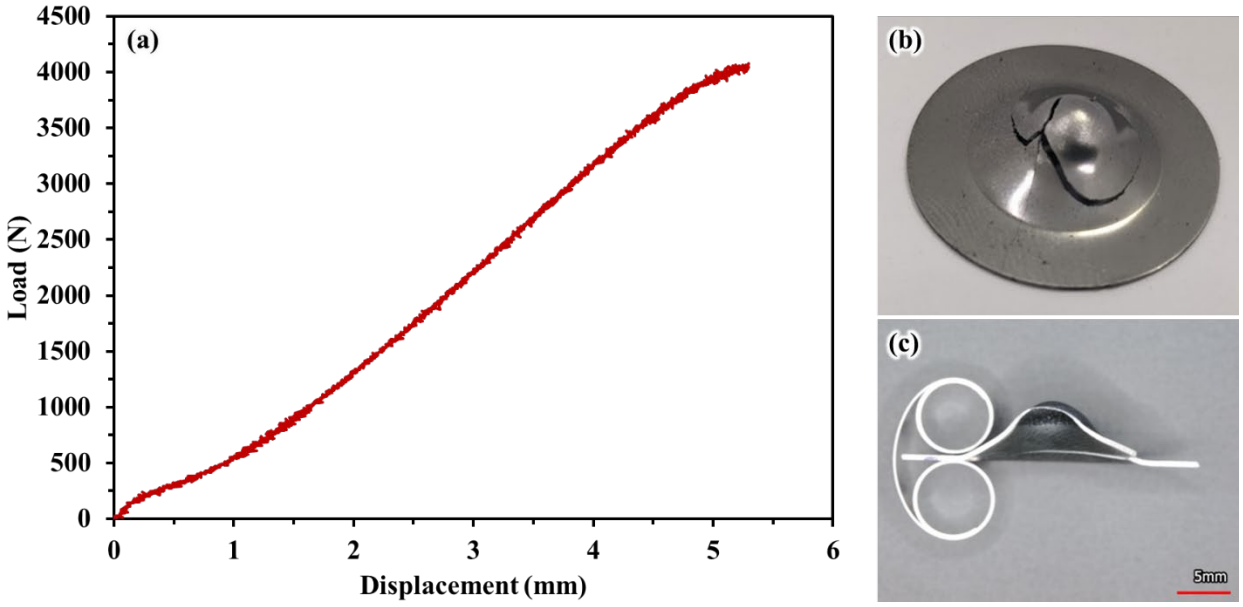

Figure 4. (a) Load vs. displacement curve recorded during SPT of <99% dense sheet Mo punched into a 29 mm OD disk. (b) Topographical photograph and (c) cross section of the fracture surface from the punched sheet Mo.

Multiple different batches of disk samples were fabricated by Northstar's collaborator Calchemist (CC) and in-house by Oak Ridge National Laboratory (ORNL). A complete list of the samples tested are reported in Table 3. Different lubricants such as Teflon (T), stearic acid (SA), SA with subsequent wiping of the excess (SAW), and ethylene bis stearamide (EBS) were all varied between disk batches. Different pressing pressures were also tested. Except for five disks manufactured from the enriched aMo powder, all feedstock powder used for the samples were fabricated from commercially available pure Mo sources, such as HC Starck. Disks manufactured from the press and sintered method were compared with those sectioned from sheet Mo produced from more conventional routes. The sheet Mo is expected to have a part density of >99%, whereas the density of the press and sintered disks will all be <99%. Porosity from the press and sinter method aid in target dissolution after being subjected to the accelerator, whereas a fully dense target, such as those produced from sheet Mo and other more conventional methods, are more difficult to dissolve, increasing the corrosivity of the dissolution bath and the time needed to achieve full dissolution. Despite this, some higher density (HD) samples were fabricated to help increase the strength—and possibly the ductility—of the Mo targets.

Table 3. SPT properties and derived tensile properties from the SPT for various Mo disks fabricated under different conditions.

									Torres et al.		Based on Mo data		
No.	**Place pressed**	**Lube**	**Press. (ksi)**	**%TD**	**t (mm)**	**$P_{t/10}$**	**P_M**	**δ_M**	**YS**	**UTS**	**YS**	**UTS**	**Elongation (%)**
210221-6	CC	T	100	85.8	0.513	156.00	247.24	2.63	240.53	169.59	273.60	102.23	13.41
210221-7	CC	T	100	87.6	0.509	138.00	241.50	2.21	221.21	176.95	229.60	117.83	12.07
210221-8	CC	T	100	87.3	0.533	91.00	204.21	0.82	152.96	235.85	74.19	242.79	7.32
210221-9	CC	T	100	87.2	0.596	97.00	211.38	2.28	137.78	163.14	39.61	88.54	11.21
210221-10	CC	T	100	87.5	0.51	78.00	234.33	2.14	146.40	176.87	59.24	117.66	11.84
Avg.				87.08	0.53	112.00	227.73	2.02	179.78	184.48	135.25	133.81	11.17
Dev.				0.66	0.03	29.78	16.94	0.62	42.44	26.19	96.64	55.57	2.05
210221-66	CC	SA	225	95.2	0.461	144.00	179.82	0.37	267.79	369.75	335.67	526.84	6.10
210221-67	CC	SA	225	95.7	0.469	111.00	179.82	1.29	212.20	196.24	209.09	158.76	9.37
210221-68	CC	SA	225	95.8	0.471	172.00	176.96	0.33	299.20	392.21	407.21	574.49	5.91
210221-69	CC	SA	225	95.9	0.476	118.00	208.51	2.42	217.40	169.09	220.92	101.17	13.33
210221-70	CC	SA	225	95.5	0.539	115.00	174.09	1.15	177.24	192.30	129.47	150.41	8.34
Avg.				95.62	0.48	132.00	183.84	1.11	234.77	263.92	260.47	302.33	8.61
Dev.				0.25	0.03	23.11	12.52	0.76	43.27	96.29	98.54	204.27	2.71
210221-76	CC	T	225	96.2	0.468	134.00	212.81	1.53	246.65	196.06	287.53	158.39	10.26
210221-77	CC	T	225	96.2	0.466	128.00	191.30	0.71	239.46	261.84	271.16	297.94	7.30
210221-78	CC	T	225	96.1	0.579	145.00	168.35	2.56	189.03	153.45	156.31	67.98	12.20
210221-79	CC	T	225	95.7	0.647	181.00	194.17	0.46	188.98	279.63	156.21	335.67	5.92
210221-80	CC	T	225	95.9	0.535	134.00	169.78	0.51	200.48	272.03	182.40	319.55	6.33
Avg.				96.02	0.54	144.40	187.28	1.15	212.92	232.60	210.72	235.91	8.40
Dev.				0.19	0.07	19.11	16.61	0.80	25.06	49.44	57.07	104.88	2.43
210221-86	CC	T	225	94.4	0.482	85.00	131.06	0.40	167.60	284.80	107.53	346.64	6.13
210221-87	CC	T	225	94.4	0.471	100.00	148.27	1.45	194.89	177.32	169.67	118.63	9.95
210221-88	CC	T	225	94.1	0.48	88.00	202.77	1.72	172.77	184.03	119.30	132.86	10.80
210221-89	CC	T	225	94.2	0.476	69.00	194.17	1.14	147.89	210.36	62.64	188.71	8.77
210221-90	CC	T	225	93.8	0.49	79.00	225.72	1.24	155.76	213.31	80.57	194.97	9.01
Avg.				94.18	0.48	84.20	180.40	1.19	167.78	213.96	107.94	196.36	8.93
Dev.				0.22	0.01	10.23	35.25	0.44	16.12	38.13	36.72	80.89	1.58
210221-96	CC	SA-W	225	94.2	0.462	97.00	228.59	2.88	196.07	166.92	172.36	96.58	15.29
210221-97	CC	SA-W	225	93.8	0.474	154.00	273.06	0.55	270.31	369.18	341.42	525.64	6.70
210221-98	CC	SA-W	225	94.1	0.471	124.00	207.08	2.21	229.66	173.23	248.85	109.96	12.67
210221-99	CC	SA-W	225	94.1	0.453	74.00	237.20	1.88	165.91	191.68	103.68	149.10	11.76
210221-100	CC	SA-W	225	93.9	0.477	167.00	214.25	0.85	285.91	249.10	376.94	270.91	7.76
Avg.				94.02	0.47	123.20	232.03	1.68	229.57	230.02	248.65	230.44	10.84
Dev.				0.15	0.01	34.57	23.07	0.86	44.74	75.37	101.88	159.90	3.18
210221-130	ORNL	SA-W	225	93.1	0.468	181.00	438.01	1.63	315.62	260.34	444.59	294.74	10.63
210221-131	ORNL	SA-W	225	93.2	0.483	159.00	458.09	1.59	269.07	265.24	338.58	305.15	10.32
210221-132	ORNL	SA-W	225	92.8	0.474	135.00	247.24	1.73	243.13	197.00	279.52	160.39	10.91
210221-133	ORNL	SA-W	225	93.3	0.459	157.00	247.24	0.80	289.52	282.82	385.16	342.44	7.69
Avg.				93.10	0.47	158.00	347.64	1.44	279.33	251.35	361.96	275.68	9.89
Dev.				0.19	0.01	16.28	100.65	0.37	26.63	32.47	60.64	68.89	1.29
210221-146*	CC	T	225	89.1	0.474	234.00	366.29	1.58	384.75	240.87	602.02	253.45	10.36
210221-147	CC	T	100	84.2	0.532	188.00	294.57	2.28	263.50	183.52	325.92	131.79	11.97
Avg.				86.65	0.50	211.00	330.43	1.93	324.13	212.20	463.97	192.62	11.17
Dev.				2.45	0.03	23.00	35.86	0.35	60.62	28.67	138.05	60.83	0.81
210221-71	CC	CC	225	95	0.469	162.60	261.58	1.67	287.60	204.49	380.79	176.27	10.77
210221-72	CC	CC	225	91.4	0.466	186.99	313.22	1.11	326.77	267.99	469.98	310.97	8.75
210221-73	CC	CC	225	91.4	0.45	174.00	320.39	1.40	326.18	245.17	468.64	262.56	9.99
210221-74	CC	CC	225	91.1	0.44	192.00	331.86	0.94	368.76	312.80	565.60	406.03	8.36
210221-75	CC	CC	225	91.5	0.453	178.00	294.57	2.69	328.80	183.14	474.61	130.99	14.79
Avg.				92.08	0.46	178.72	304.32	1.56	327.62	242.72	471.92	257.36	10.53
Dev.				1.47	0.01	10.27	24.57	0.62	25.68	45.97	58.49	97.52	2.30
210221-81	CC	CC+EBS	225	89.7	0.441	207.00	347.64	1.97	392.10	220.11	618.76	209.40	12.28
210221-82	CC	CC+EBS	225	89.9	0.45	164.00	296.01	2.09	310.31	200.05	432.50	166.85	12.60
210221-83	CC	CC+EBS	225	89.5	0.452	141.00	280.23	0.97	271.83	276.23	344.87	328.46	8.34
210221-84	CC	CC+EBS	225	89.7	0.44	146.00	287.40	1.33	292.39	241.22	391.70	254.19	9.84
210221-85	CC	CC+EBS	225	89.8	0.449	162.00	285.97	1.41	308.28	232.16	427.88	234.96	10.03
Avg.				89.72	0.45	164.00	299.45	1.55	314.98	233.95	443.14	238.77	10.62
Dev.				0.13	0.00	23.26	24.62	0.42	40.96	25.24	93.27	53.54	1.60
220427-6	CC			HD	0.5	96	268.22	0.78	173.43	286.07	384.00	684.65	489.49
220427-8	CC			HD	0.5	83	170.69	0.92	156.72	213.13	332.00	370.63	511.30

									Torres et al.		Based on Mo data		
No.	**Place pressed**	**Lube**	**Press. (ksi)**	**%TD**	**t (mm)**	**$P_{t/10}$**	**P_M**	**δ_M**	**YS**	**UTS**	**YS**	**UTS**	**Elongation (%)**
220427-24	CC			HD	0.5	93	192.20	0.67	169.57	261.18	372.00	577.50	494.52
220427-25	CC			HD	0.5	92	206.54	0.69	168.29	267.06	368.00	602.81	496.20
					0.5	91	209.41	0.76	167.00	256.86	364.00	558.90	497.88
					0	4.84	36.27	0.10	6.23	26.87	19.39	115.69	8.13
220208-15	CC	aMo	N/A	N/A	0.5	215.00	331.86	2.25	860.00	294.36	469.18	157.01	12.36
220208-17	CC	aMo	N/A	N/A	0.5	197.00	274.49	2.03	788.00	269.94	416.49	144.97	11.61
220208-18	CC	aMo	N/A	N/A	0.5	226.00	329.00	1.99	904.00	330.73	501.39	174.93	11.46
220208-49	CC	aMo	N/A	N/A	0.5	185.00	231.46	1.90	740.00	243.50	381.36	131.94	11.17
220208-50	CC	aMo	N/A	N/A	0.5	257.00	287.40	0.48	1028.00	1206.29	592.14	606.41	6.34
Avg.						216.00	290.84	1.73	864.00	468.97	472.11	243.05	10.59
Dev.						24.92	37.27	0.64	99.66	369.78	72.94	182.23	2.16
S25-1	ORNL	EBS	127	N/A	0.5	148.00	458.09	1.17	240.28	308.69	273.03	397.31	8.69
S25-2	ORNL	EBS	127	N/A	0.5	179.00	534.11	1.29	280.14	319.47	363.79	420.18	9.09
S25-3	ORNL	EBS	127	N/A	0.5	155.00	545.58	1.30	249.28	322.49	293.53	426.59	9.12
S25-4	ORNL	EBS	127	N/A	0.5	138.00	409.32	1.02	227.43	313.60	243.76	407.73	8.18
S25-5	ORNL	EBS	127	N/A	0.5	186.00	601.52	1.34	289.13	335.04	384.28	453.22	9.28
S25-6	ORNL	EBS	127	N/A	0.5	175.00	600.09	1.34	274.99	334.93	352.08	452.97	9.27
S25-7	ORNL	EBS	127	N/A	0.5	159.00	693.32	1.46	254.42	348.19	305.24	481.11	2.91
Avg.						162.86	569.96	1.29	259.05	330.85	315.78	444.32	7.75
Dev.						16.30	93.30	0.15	21.34	11.85	48.59	25.14	2.45
S50-1	ORNL	EBS	127	N/A	0.5	247.00	481.04	1.21	363.36	310.81	553.32	401.82	8.79
S50-2	ORNL	EBS	127	N/A	0.5	161.00	522.63	1.28	256.99	316.14	311.09	413.12	9.07
S50-3	ORNL	EBS	127	N/A	0.5	237.00	607.26	1.34	354.70	337.79	533.59	459.06	9.26
S50-4	ORNL	EBS	127	N/A	0.5	163.00	275.93	0.71	259.57	308.26	316.95	396.39	7.12
S50-5	ORNL	EBS	127	N/A	0.5	151.00	501.12	1.41	244.14	291.88	281.82	361.66	9.51
S50-6	ORNL	EBS	127	N/A	0.5	205.00	532.67	3.47	313.56	198.34	439.91	163.22	16.48
Avg.						194.00	487.92	1.64	285.79	290.48	376.67	358.69	10.29
Dev.						38.03	111.86	0.95	41.88	48.38	95.38	102.64	3.21
AA-1	Sheet Mo	N/A	N/A	>99	0.5	475.00	5072.35	4.59	660.67	640.12	1230.36	1100.41	20.29
AA-2	Sheet Mo	N/A	N/A	>99	0.5	326.00	4300.67	5.17	469.12	513.31	794.15	831.40	22.25
AA-3	Sheet Mo	N/A	N/A	>99	0.5	265.00	2976.78	4.41	390.70	440.90	615.56	677.79	19.65
AA-4	Sheet Mo	N/A	N/A	>99	0.5	214.00	4039.63	4.90	325.13	510.05	466.26	824.48	21.33
AA-5	Sheet Mo	N/A	N/A	>99	0.5	263.00	2493.41	4.07	388.13	411.84	609.71	616.14	18.50
AA-6	Sheet Mo	N/A	N/A	>99	0.5	197.00	4092.70	5.34	303.28	483.30	416.49	767.73	22.81
Avg.						290.00	3580.64	4.78	375.27	471.88	580.43	743.51	20.91
Dev.						92.47	712.47	0.47	58.15	39.67	132.42	84.15	1.61

Select load vs. displacement curves are shown in Figure 5. Curves for the S25 samples pressed at ORNL, from which the Mo data calibration is partly derived, are shown in Figure 5(a) and have a behavior similar to the expected loading curve shown in Figure 3(a) or the sheet Mo shown in Figure 4(a). Moreover, all the curves are fairly consistent. In comparison, some other powder batches shown in Figure 5(b) and Figure 5(c) did not show ideal behavior as desired, and the P_M varied, causing a larger deviation between samples. The multitude of local maxima are a result of continued loading and cracking in the sample. Whereas only one failure was observed in the sheet Mo that dropped the load significantly. Loading curves for the aMo samples are shown in Figure 5(d) and are more consistent than some of the pure Mo counterparts. Although an elastic region is difficult to determine in the aMo curves, the loading behavior is clearer with typically only one fracture at the P_M.

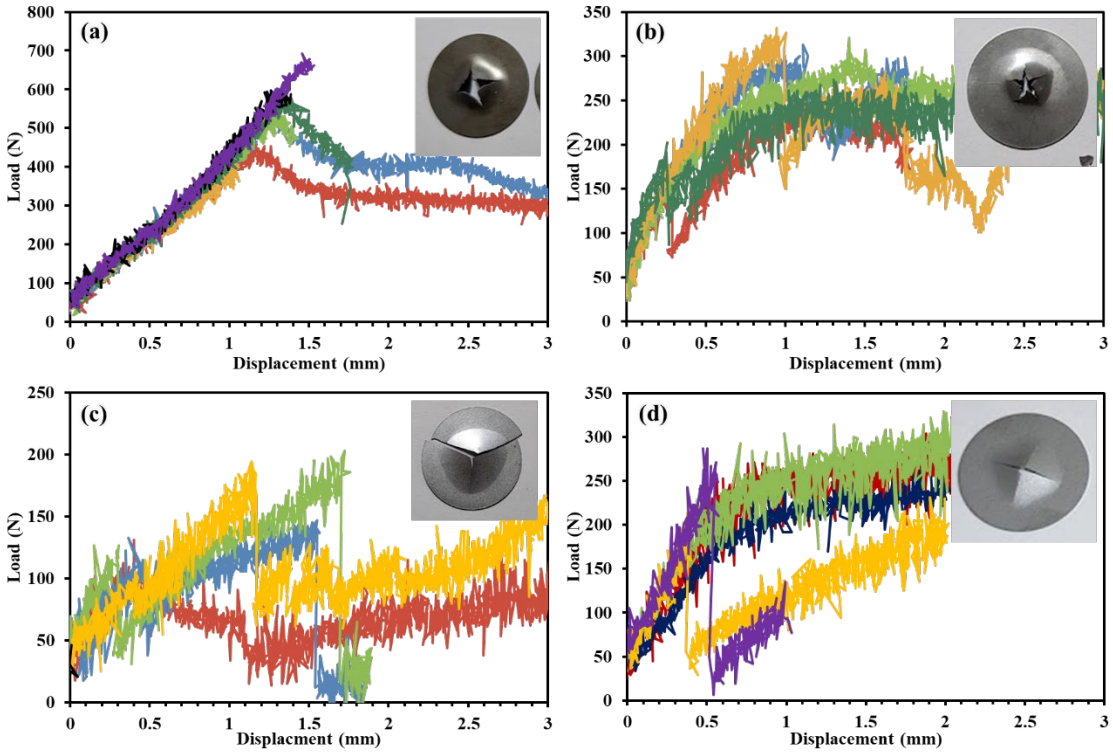

Figure 5. Load vs. displacement curves from (a) ORNL-25, (b) CC-T, (c) CC-EBS, and (d) aMo samples. Full details on these materials are provided in Table 3.

3.2 RELATING SPT TO TENSILE PROPERTIES

Typical properties measured from a tensile test of a dog-bone sample include the YS, in which the samples translate from elastic to plastic behavior; the UTS; and the total elongation to failure. Multiple studies have subjected low-temperature commercial alloys such as stainless steel (SS) 316, SS304, Inconel 625, Inconel 718, and AA6061. These alloys have good ductility at room temperature and will exhibit a typical deformation and fracture behavior, as shown in Figure 3. Once tested, the values for $P_{t/10}$ P_M, and δ_M are extracted and can be related the YS and UTS from the following expressions:

$$\mathrm{YS} = \mathrm{a}\frac{\mathrm{P_{t/10}}}{\mathrm{t^2}} + \mathrm{b}, \tag{1}$$

$$\mathrm{UTS} = \mathrm{c}\frac{\mathrm{P_M}}{\mathrm{\delta_M t}} + \mathrm{d}. \tag{2}$$

In Eqs. (1) and (2), the values of *a*, *b*, *c*, and *d* are constants derived from fitting the left side of the equation to the right side. In a comprehensive review [13], the values of *a*, *b*, *c*, and *d* were derived from multiple SPT data sources across many commercial alloys using simple linear regression between the tensile and SPT properties. Although the dataset appears comprehensive, few studies exist on applying the SPT to refractory materials, such as Mo, that do not perform the same as Fe- or Ni-based alloys. Therefore, values for *a*, *b*, *c*, and *d* are unlikely to translate.

Disks fabricated by ORNL—labeled as S25, S50, and AA (sheet Mo)—were produced, and subsize tensile specimens were machined from the disks. The subsized samples were tested with an MTS tensile-

compressive load frame with a similar controller as was used for the SPT samples. Values for the YS, UTS, and elongation were extracted from the tensile stress-strain curves and were plotted against their SPT counterparts in Figure 6(a) and are reported in Table 4. Based on the three data points, a linear regression was fitted to determine the calibration constants *a*, *b*, *c*, and *d* that are likely more appropriate for the Mo samples. Measuring the $P_{t/10}$ was difficult because there was no clear elastic region and the line drawing had to be performed manually. Therefore, the YS calculated may be inaccurate and should be taken as only a general estimate that likely does not compare between samples.

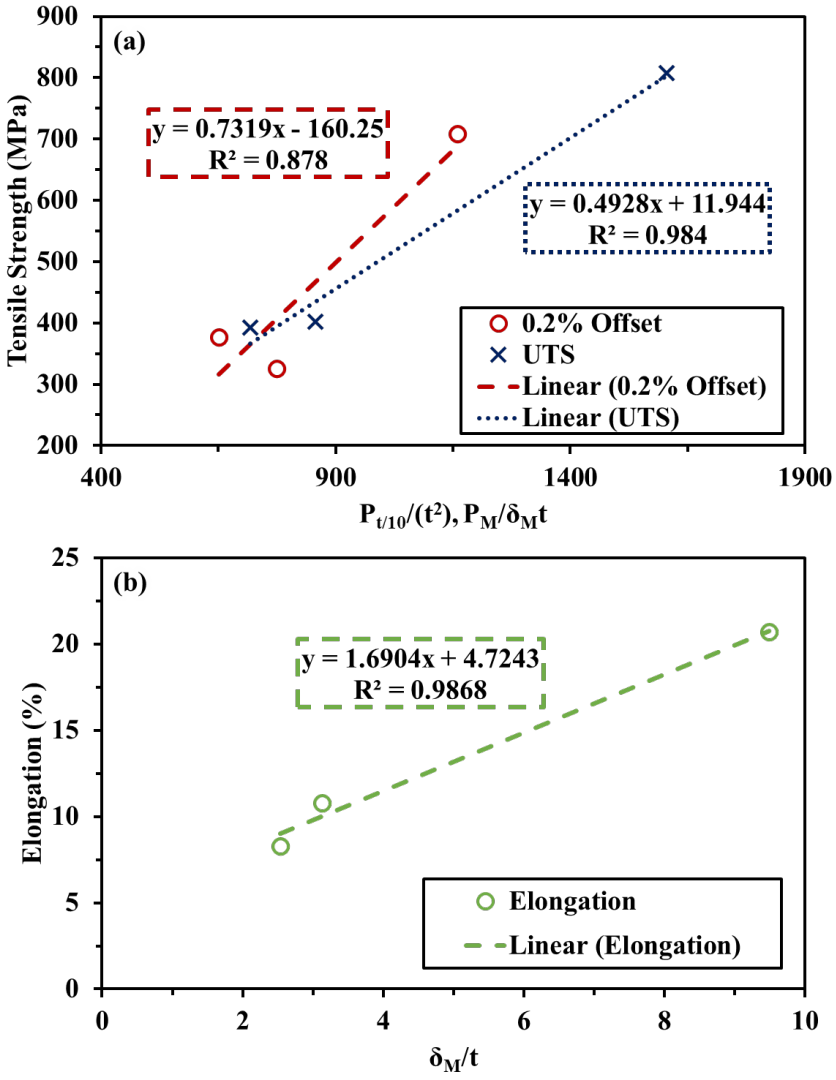

Figure 6. Fitted calibration curves relating SPT to tensile properties. The linear regression fitting was used to calibrate the Mo samples along with those proposed in Torres et al. [13] for lower temperature commercial alloys.

Table 4. SPT and tensile values for the S25, S50, and sheet Mo disks produced at ORNL. Tensile properties were calculated from stress-strain curves produced from subsize specimens machined from 29 mm disks.

	$P_{t/10}/t^2$ (N)	$P_M/\delta_M t$	δ_M/t	YS (MPa)	UTS (MPa)	Elongation (%)
S25	651.43	856.77	2.54	377.33	402	8.3
S50	77.83	718.21	3.13	326	393	10.8
Mo sheet	1,160	1,605.21	9.49	708	808	20.7

Aside from the YS and UTS, the tensile elongation is typically extracted from the fracture surface analysis. The fracture surface of the sheet Mo disk is shown in Figure 4(b) and Figure 4(c). As shown previously in Figure 3(b) and Figure 3(c), the typical fracture surface of a ductile sample should exhibit a protruded nose, which was observed in the sheet Mo samples in Figure 4(b) and Figure 4(c). The tensile elongation can be estimated by comparing the final thickness (*tf*) in the region with highest deformation with that of the original thickness:

$$\varepsilon = \ln\left(\frac{t}{t_f}\right). \quad (3)$$

The fracture surfaces of some of the pressed and sintered disks are shown as insets in Figure 5. Overall, the samples showed some deformation with some resemblance of the protruded nose. However, the samples all appeared to fail under brittle fracture because there was minimal plasticity and only cracking. Many samples were reduced to small pieces near the fracture surface, making it difficult to measure the t_f. Therefore, the relationship between the t and δ_M can be applied to estimate the tensile elongation [16]:

$$\text{Elongation} = e\frac{\delta_M}{t} + f. \quad (4)$$

Similar to Eqs. (1) and (2), calibration constants e and f can be derived from simple regression fitting, as performed in Figure 6(b). Values for the calibration constants taken from the Mo data are compared with data reported in Torres et al. in Table 1 [13].

Table 5. Calibration constants used to relate SPT to tensile properties as calculated from Mo data and that reported by Torres et al. and Garcia et al. for lower temperature melting alloys [13, 16].

Mechanical property	Fitting parameter 1 (a, c, e)		Fitting parameter 2 (b, d, f)	
	Torres et al./ Garcia et al.	Mo data	Torres et al./ Garcia et al.	Mo data
YS (MPa)	0.3214	0.7319	50.013	–160.25
UTS (MPa)	0.2323	0.4928	127.03	11.944
Elongation (%)	6.07	1.694	0	4.7243

Using the calibration constants in Table 5 and Eqs. (1) and (2), the YS and UTS were calculated from the SPT data for the various sample batches, as shown in Figure 7. Overall, the calibration constants from Torres et al. [13] tended to have lower YS and UTS values over those calibration constants produced from the Mo data. For example, the YSs of the sheet Mo calculated from Torres et al. [13] and from Mo data were 423 and 689 MPa, respectively. The tensile YS of the sheet Mo was 708 MPa. Although the derivation from the Mo data forces a fitting of the YS through only three data points based on sheet Mo, S25, and S50, one being the sheet Mo, the Torres et al. [13] fitting is clearly not proper. Although it may be backed by a large data library, the lower melting temperature alloys do not perform the same as refractories, including Mo.

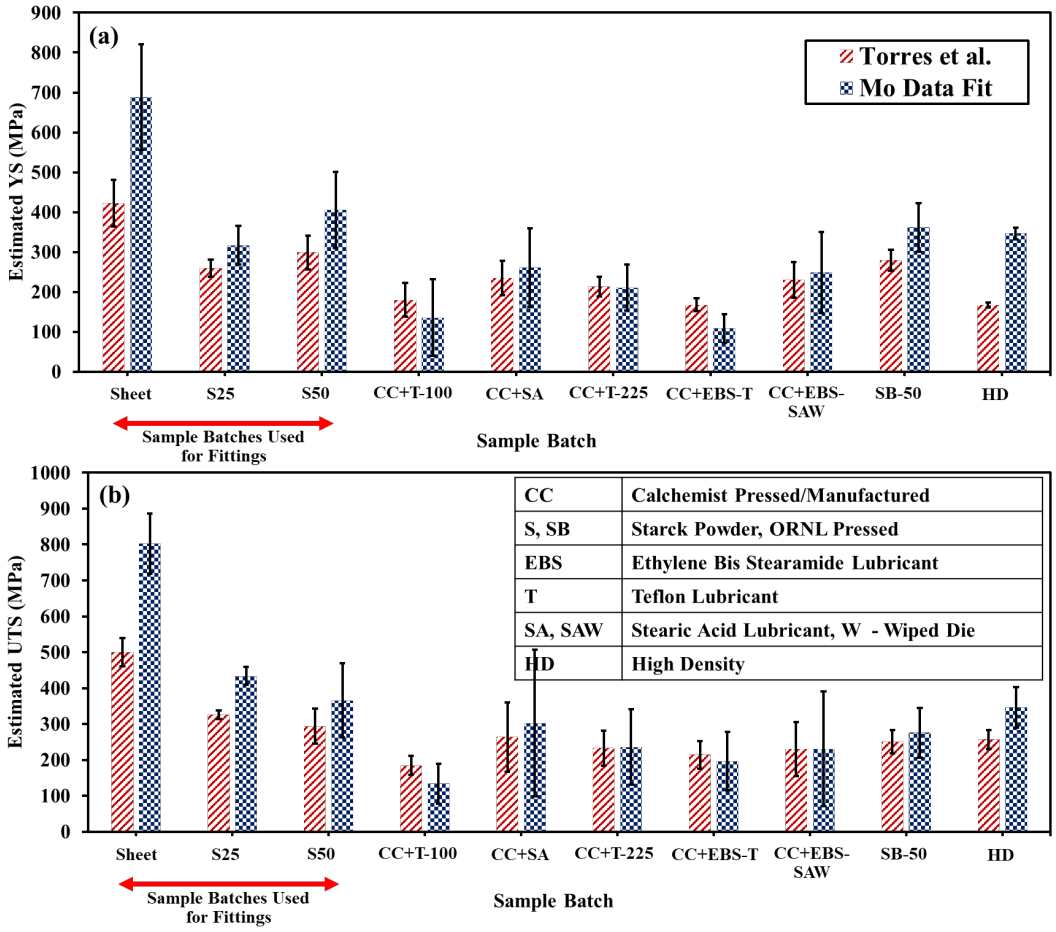

Figure 7. Comparison of the calculated (a) YS and (b) UTS for the various Mo disk batches derived from calibration constants reported in Torres et al. [13] and produced from the Mo data.

For a more condensed view of the calculated tensile properties, the YS, UTS, and elongation calculated using Mo data calibration constants is shown in Figure 8. The standard deviation of the values is larger than preferred and is a result of poor consistency between samples in the same batch. An estimate of the tensile elongation appeared to ~10% but is not indicative of the real uniform elongation. Equation (4) was proposed as a method for estimating elongation for brittle samples, but there is not yet enough data to suggest that it is an accurate value. The ORNL-produced samples performed slightly higher than the CC-fabricated samples but were still lower than those from the sheet Mo. A few HD samples were also tested and yielded strengths similar to the ORNL S25 and S50, so HD may have helped the sample take more load.

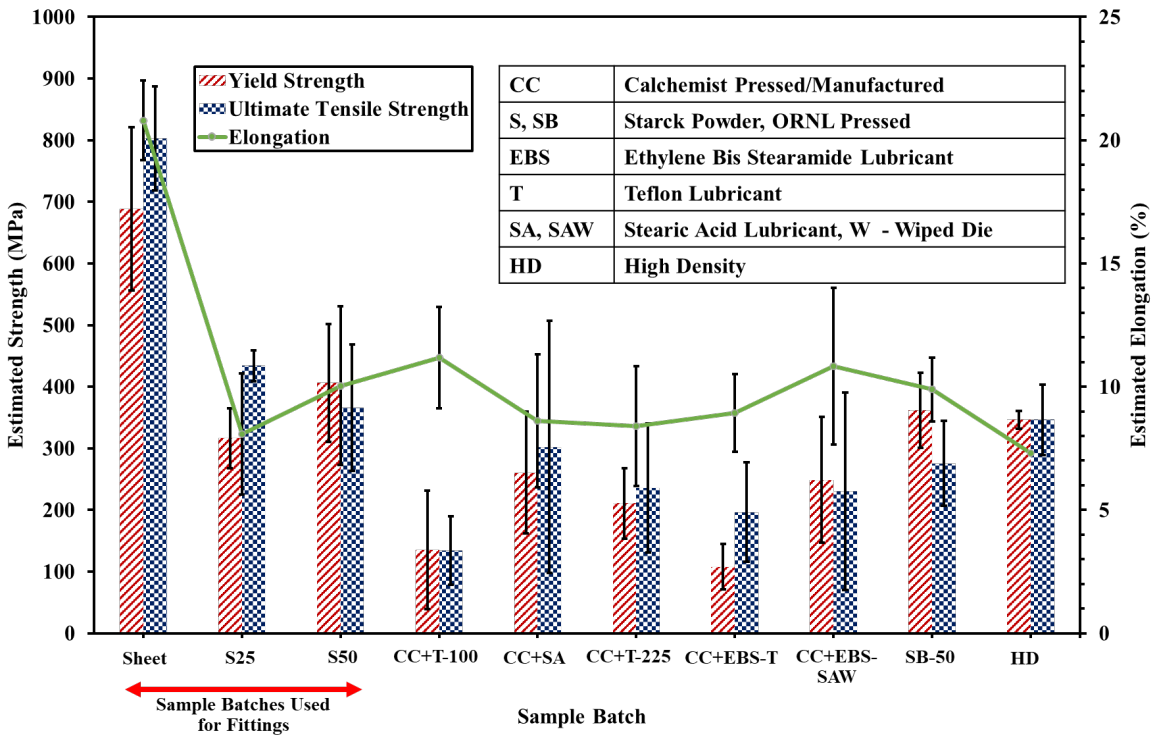

Figure 8. Tensile properties derived from SPT using calibration constants taken from Mo data.

In addition to the disks pressed from commercially available powder, some disks were tested using the enriched aMo powder. The YS, UTS, and elongation were calculated based on the Mo data calibration constants and are shown in Figure 9. Additional disks were subjected to multiple sintering cycles, indicated by *3*×, *4*×, *5*×, and *6*×, which represents the number of times they were cycled. Multiple cycling was performed to help grow grains and increase ductility. Again, the YS and elongation values are somewhat unreal because it was difficult to distinguish an elastic region, and most samples had a brittle fracture, making it too difficult to measure a final thickness near the fracture surface. Observations of the UTS, which is derived based on the P_Y and t, indicate that the samples all performed similarly and exhibited lower strengths than what was observed in Figure 8 for their pure Mo counterparts.

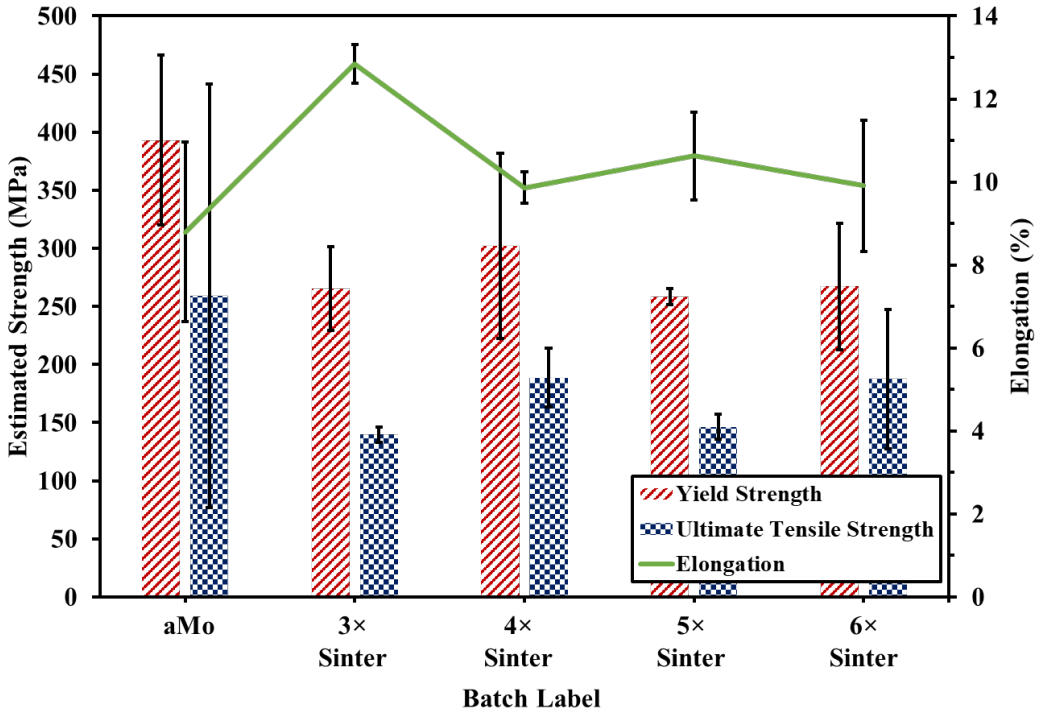

Figure 9. Calculated tensile properties derived from SPT using calibration constants taken from Mo data for the aMo samples. The reference to 3x, 4x, 5x, 6x, sintered were disks subjected to multiple sintering cycles.

Although the SPT results indicate highs and lows in different samples, the estimate given for the tensile properties is not analogous to the properties measured from testing a similar sample in tension. Studies such Leclerc et al. [15] have shown SPT sensitivity regarding alloys and processing methods. Therefore, more data are needed to improve the calibration curves shown in Figure 6. Future studies are warranted to continue testing various Mo samples with SPT vs. tensile to tune the accuracy of the SPT.

4. SUMMARY AND FUTURE OUTLOOK

The SPT was designed to provide a method for Northstar to test their pressed and sintered disk-shaped targets for quality assurance. This report provides data and analyses to show the initial and ongoing development of the SPT for use in helping Northstar mechanically assess its targets; however, this information does not yet equilibrate to true tensile/compressive loading. Correlating tensile properties of the disks to the SPT data was difficult because reported literature values are based on studies that used lower temperature—mostly Fe and Ni—alloys. Because Mo is a high melting temperature refractory material, the SPT to tensile calibration constants used need to be derived from refractory material. Few studies exist on testing refractories with SPT, so calibration constants were derived from performing tensile testing on subsize specimens fabricated at ORNL. Sheet Mo and two other disk batches were the only samples tested in tension at the time and therefore are the sole three data points used in each calibration curve. A general estimate of the UTS could be calculated, but the disks failed under brittle fracture, making it difficult to determine an elastic region for calculating a YS or estimating the elongation taken by relating the initial thickness to the final thickness in the fracture surface. Therefore, more data and evaluations are needed before the SPT can be better understood and applied in quality assurance testing for Mo targets.

5. REFERENCES

[1] R.G. Bennett, J.D. Christian, D.A. Petti, W.K. Terry, S.B. Grover, "A System of 99 M Tc Production Based on Distributed Electron Accelerators and Thermal Separation", *Nucl. Technol.* 126(1) (1999) 102-121,

[2] J. McCarter, J. Harvey, M. Brennan, S. Burns, S. Kelley, T. Montenegro, Q. Schiller, "Accelerator Production of Mo-99 Using Mo-100", (2021),

[3] T.J. Ruth, "The Shortage of Technetium-99m and Possible Solutions", *Annual Review of Nuclear and Particle Science* 70 (2020) 77-94,

[4] K.A. Woloshun, G.E. Dale, E.R. Olivas, A.C. Naranjo, F.P. Romero, "29 Mm Diameter Test Target Design Report", Los Alamos National Lab.(LANL), Los Alamos, NM (United States)(2016), LA-UR-16-27128

[5] K.A. Woloshun, G.E. Dale, E.R. Olivas, F.P. Romero, D.A. Dalmas, S. Chemerisov, R. Gromov, R. Lowden, "Thermal Test on Target with Pressed Disks", United States, (2016), 10.2172/1245565

[6] R.A. Lowden, S. Nunn, J. Kiggans Jr, R.J. Parten, C. Bryan, "Powder Metallurgy Fabrication of Molybdenum Accelerator Target Disks", (2015), ORNL/TM-2014/238

[7] R.A. Lowden, E. Lara-Curzio, W.D. Porter, H. Wang, "Thermophysical Properties of Powder Metallurgy Molybdenum Target Materials", Oak Ridge National Laboratory(2015), ORNL/TM-2014/629

[8] P. Tkac, G.F. Vandegrift, J. Harvey, "Dissolution of Sintered Mo Disks", Argonne National Lab.(ANL), Argonne, IL (United States)(2013), ANL/CSE-13/19

[9] R.A. Lowden, J. J. O. Kiggans, S.D. Nunn, F. Montgomery, P. Menchhofer, C.D. Bryan, "Large-Batch Reduciton of Molybdenum Trioxide", Oak Ridge National Laboratory(2015), ORNL/TM-2014/630

[10] S. Chemerisov, J. Bailey, T. Heltemes, C. Jonah, V. Makarashvili, P. Tkac, D. Rotsch, M. Virgo, G. Vandegrift, "Results of the Six-and-a-Half Day Electron-Accelerator Irradiation of Enriched Mo-100 Targets for the Production of Mo-99", Argonne National Lab.(ANL), Argonne, IL (United States)(2016),

[11] R.A. Lowden, R.G. Miller, C.D. Bryan, "Laser Heating of Target Disks to Assess Potential in-Accelerator Distortion", Oak Ridge National Laboratory(2014), ORNL/TM-2014/626

[12] ASTM, "Standard Test Method for Small Punch Testing of Metallic Materials", E3205-20, (2020),

[13] J. Torres, A.P. Gordon, "Mechanics of the Small Punch Test: A Review and Qualification of Additive Manufacturing Materials", *Journal of Materials Science* 56(18) (2021) 10707-10744,

[14] A. Janča, J. Siegl, P. Haušild, "Small Punch Test Evaluation Methods for Material Characterisation", *J. Nucl. Mater.* 481 (2016) 201-213,

[15] N. Leclerc, A. Khosravani, S. Hashemi, D.B. Miracle, S.R. Kalidindi, "Correlation of Measured Load-Displacement Curves in Small Punch Tests with Tensile Stress-Strain Curves", *Acta Mater.* 204 (2021) 116501, https://doi.org/10.1016/j.actamat.2020.116501
[16] T.E. García, C. Rodríguez, F.J. Belzunce, C. Suárez, "Estimation of the Mechanical Properties of Metallic Materials by Means of the Small Punch Test", *J. Alloys Compd.* 582 (2014) 708-717, https://doi.org/10.1016/j.jallcom.2013.08.009